Volume 1 | Number 1 | Jan 2013 | Pages 1–100

Journal of
Materials Chemistry A

Materials for energy and sustainability
www.rsc.org/materialsA

Li⁺

ROYAL SOCIETY
OF CHEMISTRY

ROYAL SOCIETY
OF CHEMISTRY

www.rsc.org/materialsA

Journal of
Materials Chemistry A

ARTICLE

Grafting of a redox polymer onto carbon nanotubes for high capacity battery materials

Bruno Ernould,[a] Marine Devos,[a] Jean-Pierre Bourgeois,[a] Julien Rolland,[a] Alexandru Vlad[a,b] and Jean-François Gohy[a]*

In this contribution we disclose an original strategy towards dense grafting of electrochemically active nitroxide-bearing polymer brushes on multi-walled carbon nanotubes (MWCNTs). Our strategy involves the surface initiated polymerization of 2,2,6,6-tetramethylpiperidin-4-yl methacrylate (TMA) through atom transfer radical polymerization from the high-density initiator functionalized surface of MWCNTs, leading to MWCNT-g-PTMA composites. Extended chemical and morphological analysis confirmed the compact core-shell morphology with high active material mass loading of 60 wt.%. The electrodes made out of these MWCNT-g-PTMA composites display good cycling stability (87% of capacity retention after 200 cycles), good rate capabilities and an excellent specific capacity (85% of the theoretical capacity). The success of this strategy offers new opportunities to overcome the issue of the PTMA solubilization through the electrolyte and minimal amount utilization of conductive carbon species.

Introduction

According to current previsions our mobile society will have to face up an ever-increasing demand for portable energy sources.[1] Li-ion batteries (LIB) are considered as the most mature technology to address the current demands for portable energy sources such as electronic devices, electric and hybrid vehicles and can be also useful for small to medium scale grid storage.[2, 3] Nevertheless the ever-growing market of LIB relies mostly on inorganic mineral materials, that suffer from limited resources.[1]

However many alternatives have been proposed over the past few years to achieve a more sustainable development.[2] Positive electrode materials based on stable organic radicals have attracted vivid interest as potential alternatives.[4] The most promising candidates of this emerging class are macromolecular architectures bearing persistent TEMPO radicals as side-chains, such as poly(2,2,6,6-tetramethylpiperidin-1-oxyl-4-yl methacrylate) (PTMA), that act as reversible redox centers.[5] PTMA benefits from several interesting features such as high electrochemical potential (3.6 V $vs.$ Li/Li$^+$), synthesis from potentially renewable sources and high stability upon cycling.[4, 6] Another key characteristic of PTMA is its high charge/discharge rate capabilities allowing

fast charges in the minute time scale,[7-9] outperforming classical intercalation transition metal oxides.

Despite, the performances of batteries based on PTMA are hindered by some of its intrinsic properties. Indeed PTMA displays a limited electrical conductivity[4, 10] and is soluble in common LIB electrolytes.[11] The common approach to improve electrical transport and charge collection in PTMA electrodes involves incorporation of conductive additives (graphite powders, carbon fibers…).[10, 12] The drawback of these methods is that conductive additives usually account for a major part in the cathode (60 to 80 wt.%),[4] considerably decreasing the specific capacity of PTMA-based electrodes.. It should be noted that carbon additives are also taking part of the formulation as adsorbant to diminish the solubilization of the active material further explaining their high content. Although providing better capacity retention, the adsorption on carbon is not irreversible and cannot avoid long-term capacity fading.[13]

To overcome these limitations, several strategies have been developed in the literature, such as cross-linking of the polymer,[6, 13, 14] surface grafting from an insoluble substrate such as silica particles,[15] utilization of nanostructured block copolymers based on PTMA blocks and insoluble phase segregated polystyrene blocks…[16]

The strategy we have explored in the present contribution consists in grafting PTMA on multi-wall carbon nanotubes

This journal is © The Royal Society of Chemistry 2015

J. Mater. Chem. A, 2015, 00, 1-3 | 1

(MWCNTs). In such a design, MWCNTs act both as structural support and conducting agent.

Although a similar strategy for a nitroxide radical bearing polynorbornene derivative has been recently reported, the active material amount grafted on MWCNTs remained low, with maximum content reported of less than 30 wt.%.[17] To overcome this limitation, we propose here a grafting strategy based on surface-initiated controlled radical polymerization (SI-CRP), a class of grafting techniques that is well known to allow polymer grafted MWCNTs with a high loading of anchored material.[18, 19] Up to 60% by wt. PTMA loadings are reported here that enable much higher specific capacities for PTMA-based electrodes. Excellent cycling stability and power performances are attained using this novel approach while working at high mass loadings and active material contents.

Experimental

Synthesis procedures

Materials. CH_2Cl_2 (DCM, HPLC grade, Fisher Scientific) is passed through a SPS solvent dispenser fitted with an aluminia column. Triethylamine (Analytical reagent grade, Fischer Scientific) is distilled over CaH_2 under argon atmosphere. 3-chloroperoxybenzoic acid (mCPBA, Aldrich, 77% max) was washed with a phosphate pH 7 buffer solution. Thin multiwall carbon nanotubes NC7000 (MWCNT) were kindly provided by Nanocyl. $SOCl_2$ (99.5+%, Fisher Scientific), 1-methyl-2-pyrrolidone (ACS reagent, Acros Organics), 2-hydroxyethyl bromosisobutyrate (95%, Sigma-Aldrich) (HEBB), HNO_3 (65%, AnalaR NORMAPUR), CuCl (Aldrich, 99.999%), $CuBr_2$ (Aldrich, 99.999%), TMPM (>98%, TCI), N,N,N',N'',N"-pentamethyldiethylenetriamine (PMDETA, Aldrich, 98%), anhydrous toluene (Extra Dry, 99.85%, over molecular sieves, AcroSeal, Acros Organics), anisole (Acros Organics, 99%) and all other chemicals are used as received.

MWCNT oxidation. In a 250 mL round-bottom flask, MWCNTs (1 g) and HNO_3 65% (100 mL) are charged. The mixture is stirred 2h at reflux (110°C). The mixture is then filtered over a PTFE 0.45 µm filter. The residue is washed with ultra pure water until filtrate reaches neutral pH. The remaining solid is dried under reduced pressure for 24 h at 35°C.

Preparation of MWCNT-COCl. A 100 mL round-bottom Schlenk flask is charged with 100 mg of previously oxidized MWCNT-COOH. The content of the flask is degassed under reduced pressure at 120°C during 4 hours. 40 mL of anhydrous toluene and 15 mL of $SOCl_2$ are then charged in the flask under argon. The MWCNTs were dispersed by immerging the Schlenk into an ultrasonic bath for 15 min. The reaction is carried out by heating at 80°C during 24 h to yield the MWCNT-COCl. The recovery is done by distillation under reduced pressure until dryness.

Preparation of MWCNT-Initiator. A 100 mL round-bottom Schlenk flask is charged under argon with 100 mg of MWCNT-COCl, 40 mL of anhydrous toluene, 5 drops of TEA and 1.8 g of HEBB. The flask is sealed and ultrasonicated during 30 min.

The functionalization is carried at 100°C during 24 h. MWCNT-initiator are recovered by filtration on 0.22 µm poly(vinylidene fluoride) (PVDF) filter and washed three times with 50 mL of toluene. The remaining solid is dried overnight under reduced pressure at 35°C.

Polymerization of TMPM via grafting from the MWCNT-initiator. In a first Schlenk flask, 28.6 mg of MWCNT-initiator (8.10^{-3} mmol of initiator groups) are charged and degassed under reduced pressure at room temperature during 3 h. Degassed anisole (10 mL) is introduced via a cannula in the vessel. The resulting mixture is then immerged in an ultrasonic bath during 30 min. TMPM (4.4 g, 19.8 mmol, 120 equiv.), $CuBr_2$ (254 µl of a solution 7.2 mg/mL in acetonitrile, 0.016 mmol, 0.1 equiv.), PMDETA (83.2 µL, 0.40 mmol, 2.42 equiv.) and anisole are charged in a Schlenk flask. This mixture is degassed by 3 freeze-pump-taw cycles and is transferred via a cannula in a 100 mL round-bottom Schlenk flask containing CuCl (16.3 mg, 0.16 mmol, 1 equiv.). The MWCNT-initiator suspension is finally added by means of a gas-tight syringe. The reaction mixture is ultrasonicated for 30 min. Polymerization takes place under argon atmosphere at 60°C during 16 h.

The reaction was quenched by cooling down quickly the medium with liquid nitrogen and exposition of the polymerization medium to air. The medium is concentrated under reduced pressure. The MWCNT-*g*-PTMPM suspension is then added dropwise to 200 mL of acetonitrile under vigorous stirring. The solid is recovered by centrifugation and resuspended in 5 mL of DCM. The dropwise addition followed by centrifugation is repeated 2 times in acetonitrile and 1 time in hexane. The remaining solid is dried overnight under reduced pressure at 35°C. This yields to 55 mg of MWCNT-*g*-PTMPM.

Oxidation of MWCNT-*g*-PTMPM into MWCNT-*g*-PTMA. In a 100 mL round-bottom flask, 45 mg of MWCNT-*g*-PTMPM (0.120 mmol of N-H moieties) and 45 mL of dry DCM are charged under argon. The flask is put in an ultrasonic bath during 15 min and subsequently thermostatized at 0°C. A solution of mCPBA (25.8 mg, 0.150 mmol, 1.25 equiv.) in dry DCM (7.5 mL) is added dropwise under stirring at 0°C during 1 h. The suspension is then stirred during the next 2 hours, while its temperature is allowed to go back to room temperature on its own accord. Afterwards the reaction medium is extracted successively twice with an aqueous solution of $NaHCO_3$ 2 % (m/m) and twice with deionized H_2O. The resulting organic phase is filtered on 0.22 µm PVDF filter and dried overnight *in vacuo* at 35°C, affording 25 mg of MWCNT-*g*-PTMA.

Characterizations

Thermogravimetric analysis. Thermograms are recorded on a TGA/SDTA 851e instrument from METTLER TOLEDO. These analyses are carried out with a heating ramp of 10°C/min and under N_2 flow (100 ml/min) with the samples (3 − 5 mg) placed into 70 µL alumina containers.

Transmission electron microscopy (TEM). TEM images are obtained with a LEO 922 OMEGA energy filter transmission electron microscope. The powder samples are suspended in

2 | *J. Mater. Chem. A*, 2015, **00**, 1-3

This journal is © The Royal Society of Chemistry 2015

dichloromethane under ultrasonic treatment, then a drop of the supernatant is deposited on a holey carbon film supported on a copper grid, which is dried overnight at room temperature before analysis.

X-ray photoelectron spectroscopy (XPS). XPS analyses are realized at room temperature by means of a SSI X-Probe (SSX 100/206) photoelectron spectrometer from FISONS equipped with a monochromatized microfocus Al X-ray source. Samples are stuck onto sample holders with double-face adhesive tape and then placed on an insulating home-made ceramic carousel (Macor®, Switzerland). The spot size for irradiation is set at 800 μm x 1200 μm. Charge effects are suppressed by placing a nickel grid above the samples and using a flood gun set at 8 eV. The energy scale is calibrated with reference to the $Au_{4f7/2}$ peak at 84 eV. Data treatment is performed with the CasaXPS program (Casa Software Ltd., UK). The peaks are decomposed into a sum of Gaussian/Lorentzian (85/15) after subtraction of a Shirley type baseline.

Electrodes design. Self-standing electrodes are produced using a vacuum filtration process over a PVDF 0.2 μm filter. The filtration device is a Millipore set-up. Pristine MWCNTs (8.0 mg) are dispersed in butanol (250 mL) using bath sonication during 30 min. This first suspension is filtered on the PVdF filter. A suspension of MWCNT-*g*-PTMA (8.0 mg in 100 mL DCM/NMP, 40:60, bath sonicated for 30 min) is then filtered over the first layer formed on PVDF (3.40 cm diameter). Electrodes are first dried in ambient air at room temperature for 2 hours, then at 60°C under vacuum for 24 hours. The resulting material is then cut in discs (1.2 cm diameter, total weight of 2.0 mg each) for electrochemical measurements.

Cell assembly. Electrodes are tested in half-cell configuration using lithium metal foil (99.9% Alfa Aesar) as reference and counter electrode. Porous polyethylene membrane was purchased from Celgard and used as separator. A mix of ethylene carbonate (EC), diethyl carbonate (DEC) and dimethyl carbonate (DMC) 1:1:1 v:v:v with 1 M of lithium

hexafluorophosphate ($LiPF_6$) was purchased from Novolyte and used as electrolyte. Cells are assembled in Swagelok cells purchased from X2Labware. All cells are assembled under argon atmosphere (<0.1 ppm H_2O, <0.1 ppm O_2) in a MBraun glovebox.

Electrochemical tests. Cyclic voltammetry (CV) and charge/discharge tests are conducted with an Arbin Instruments Battery Tester BT-2043. The electrical conductivities of the electrodes were measured by a 4-point probe station (Lucas Lab L320) coupled with a Keithley 2410 monitor. Current was adjusted to keep a constant voltage of 10 mV. Film thickness was measured using a Draper Expert digital micrometer.

Results and Discussion

Functionalization of MWCNTs into MWCNT-initiator

The grafting of polymers via surface-initiated atom transfer radical polymerization (SI-ATRP) from MWCNTs necessitates the presence of specific moieties able to initiate the polymerization.[20] To successfully graft polymers via a controlled polymerization method and to yield high polymer content onto MWCNTs, the surface of the nanotubes requires a high density of initiating groups. Since the targeted redox polymer belongs to the polymethacrylate family, we selected the bromoisobutyrate group as the initiating moiety. The selected synthetic procedure is inspired by previous works concerning SI-ATRP[18, 21, 22] and is summarized in Scheme 1. The first step consists in introducing functionality on the MWCNTs surface via chemical oxidation, leading, among others, to carboxylic acid functions. Next, the carboxylic acid functions are activated with $SOCl_2$. The accordingly generated acyl chloride subsequently reacts with the alcohol group of bromoisobutyrate, affording the MWCNT-initiator for subsequent SI-ATRP.
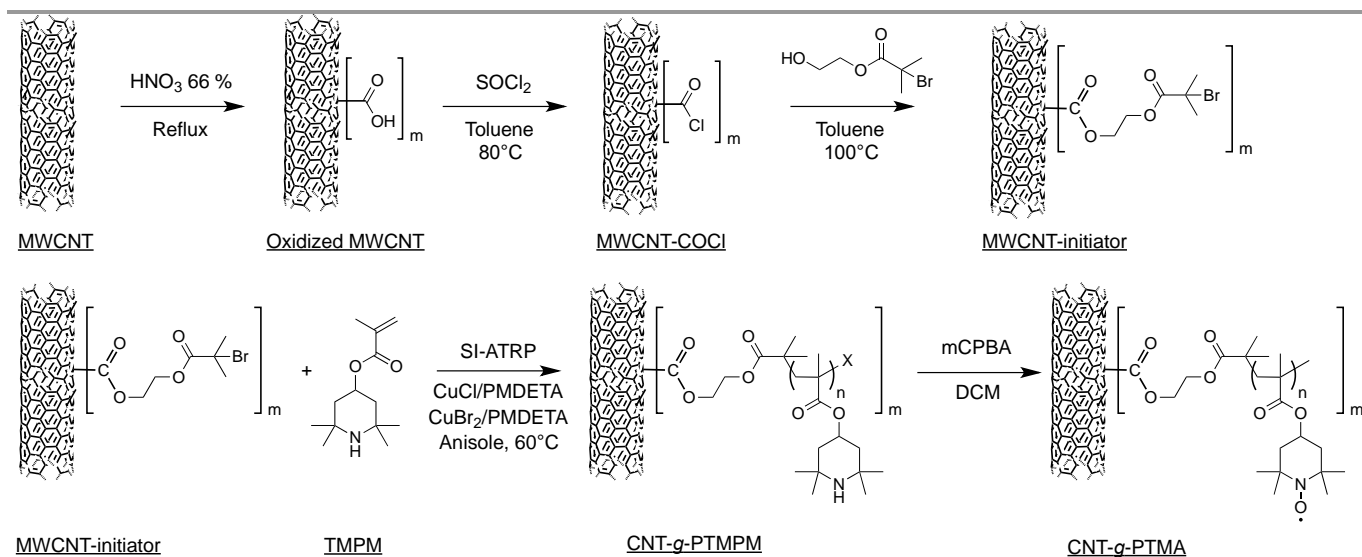
Scheme 1. Strategy for the synthesis of PTMA covalently grafted from MWCNTs.

This journal is © The Royal Society of Chemistry 2015

J. Mater. Chem. A, 2015, **00**, 1-3 | **3**

Thermogravimetric (TGA) measurements allowed us to monitor the functionalization procedure at each step. The plots for pristine MWCNTs, oxidized MWCNTs and MWCNT-initiator are displayed in Figure 1. The curves obtained for all samples are typical of such systems.[18, 19] The curve for oxidized MWCNTs displays a 4.1% weight loss between 200 and 450°C. In the same range of temperature the pristine nanotubes display a 0.7% weight loss. The increased weight loss is due to the oxidized functions introduced on the MWCNTs outer surface. In the case of MWCNT-initiator, TGA leads to a weight loss of 10% between 200°C and 450°C. The difference in weight loss (5.9%) between the oxidized MWCNT and the functionalized MWCNT is attributed to the decomposition of the initiator groups bound to the nanotubes. Calculation based on the initiator fragment molar mass (210 g.mol^{-1}) leads to a value of 4 initiating groups per 1000 carbon atoms which is in agreement with previously reported values.[21, 22]
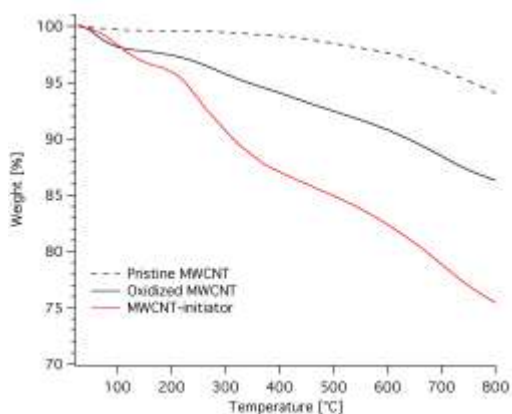
Figure 1. TGA thermograms of pristine MWCNTs, oxidized MWCNTs and MWCNTs functionalized with the ATRP initiator (MWCNT-initiator). The weight losses between 200°C and 450°C are 0.7%, 4.1% and 10% respectively.

(XPS) analyses were carried out to further assess the suitable functionalization of the MWCNTs. XPS evidences the presence of organic bromide in the MWCNTs-initiator samples considering the position of the peak (70 eV) (Br$_{3d}$ narrow scan is depicted in Supplementary Information, Figure S1). Integration of the signal yields an atomic ratio of 2 bromides per 1000 carbon atoms. This value corroborates with the TGA results further confirming proper functionalization of the MWCNTs with the SI-ATRP initiator.

PTMPM grafting from MWCNT-initiator

SI-ATRP was selected for the SI-CRP since the controlled polymerization of PTMA precursor polymer, *i.e.* poly(2,2,6,6-tetramethyl-4-piperidyl methacrylate) (PTMPM) was previously successfully demonstrated by Hauffman et al.[23] Once grafting from MWCNTs of PTMPM is achieved (yielding MWCNT-*g*-PTMPM), the later is chemically oxidized into PTMA, producing the composite cathode material (MWCNT-*g*-PTMA).

The control of the SI-ATRP process is usually achieved either by means of the addition of Cu(II) in the medium or by means

of addition of a sacrificial initiator.[20] To circumvent issues related to a possible physisorption of the growing chains onto the MWCNTs in the sacrificial approach, the polymerization was carried out by the addition of Cu(II) in the medium. The SI-ATRP set up has been adapted from previous work of our group concerning synthesis of PTMPM.[23]

The polymerization is carried out overnight at 60°C with the MWCNT-initiator (8.10^{-3} mmol of initiator groups) suspended in a TMPM solution (120 equiv. with respect to CuCl; 70 wt.% of anisole) and CuCl/CuBr$_2$/PDMETA (1/0.1/2.42 equiv./equiv./equiv.) as catalytic system.

Absence of self-initiated unbound polymer in the reaction mixture was verified by means of ^{1}H-NMR. An aliquot of the polymerization mixture is successively passed through a PTFE 0.22 μm filter and further diluted with CDCl$_3$. The analysis of this sample reveals no characteristic signals of PTMPM or other adventitious reactions.

The polymer grafted MWCNTs are highly dispersible in PTMPM compatible solvents. For example, as depicted in Figure 2, a MWCNT-*g*-PTMPM suspension in CH$_2$Cl$_2$ remains stable for more than 24 h with no sign of sedimentation while the MWCNT-initiator suspension sediments within 5 min. This experiment further emphasizes the surface modification of the nanotubes as suspensions of particles grafted with polymers are known to be stabilized when favorable interaction occurs between the grafted material and the solvent.[18, 24] When the MWCNT-*g*-PTMPM suspension is added dropwise into a larger volume of acetonitrile, particles collapse. This behavior is obviously due to the non-solvent character of acetonitrile with respect to PTMPM.

Figure 2. Suspensions (0.5 mg/mL) in CH$_2$Cl$_2$. On the left side MWCNT-initiator after 5 min rest; on the right MWCNT-g-PTMPM after 24 h rest.

To further support the efficient grafting of PTMPM onto MWCNTs, transmission electron microscopy (TEM) is used to observe an organic layer on the outer wall of the MWCNTs (Figure 3). The TEM micrographs uncover the presence of a soft material shell covering the walls of the nanotubes. Measurements obtained from several TEM micrographs lead to evaluate the average diameter of the pristine MWCNT-*g*-PTMPM to be equal to 17.3 ± 0.4 nm whereas the average diameter for pristine MWCNTs is found to be 10.9 ± 0.6 nm (Figure 3 displays the diameter distribution histogram for both samples). Hence these significantly different diameters support the evidence of an outer layer attributed to the grafted PTMPM.
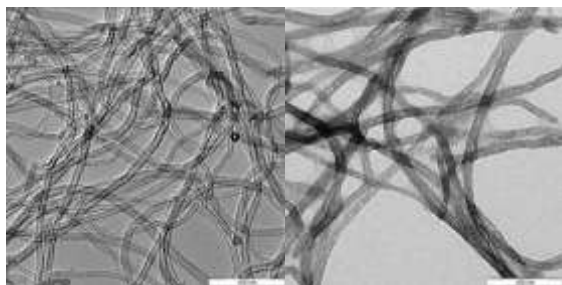
Figure 3. TEM micrographs of pristine (left) and MWCNT-*g*-PTMPM (right). Scale bars: 100 nm.
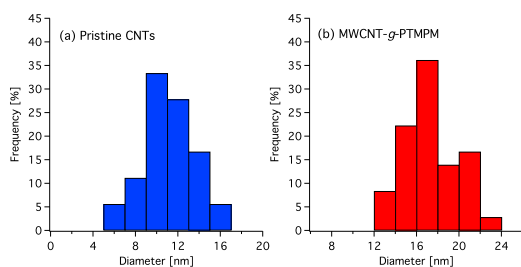
Figure 4. Diameter distribution histograms for (a) pristine nanotubes and (b) MWCNT-*g*-PTMPM. Diameters values are collected by measurements on a collection of TEM micrographs.

To confirm the nature of the MWCNTs surface modification, XPS analysis has been realized (Table 1). The MWCNT-*g*-PTMPM sample is compared to a PTMPM homopolymer. XPS analysis points out atomic concentrations for the MWCNT-*g*-PTMPM sample close to those obtained for a PTMPM sample. Seemingly, the MWCNTs signature is so efficiently screened by the polymeric shell that is not contributing to the collected signals. The C_{1s} line shape signals of MWCNT-initiator exhibits the usual characteristic tail of oxidized CNTs[25] (MWCNT-initiator, Figure 5a). In contrast, the line shape for MWCNT-*g*-PTMPM presents a main peak with a shoulder (Figure 5c) and the general aspect is more typical of the pure PTMPM sample. These observations tend to demonstrate that a uniform polymer shell efficiently masks the MWCNT core. Moreover the O/C and N/C ratios are fairly matching the ratios that could be predicted based on the PTMPM chemical composition (Table 1).

Table 1. Experimental surface atomic concentrations for MWCNT-*g*-PTMPM compared to experimental and predicted values for pure PTMPM.

Spectral line	Surface atomic concentrations (%)		
	MWCNT-*g*-PTMPM	PTMPM	
	Found	Found	Expected
C_{1s}	83.0	82.4	81.3
O_{1s}	11.7	11.8	12.5
N_{1s}	5.2	5.8	6.3

The determination of the polymeric fraction of the MWCNT-*g*-PTMPM is performed again by means of TGA (Figure 6). A considerable mass loss can be seen on the curves of the composite sample around 300°C. This drop can be ascribed to

the grafted polymer degradation occurring in the same range of temperature as the pure PTMPM sample. The analyses lead to a polymeric content as high as 60% (Figure 6). Considering the number of initiating groups per gram of CNTs and an initiator efficiency of 70% close to the value obtained for similar initiator moieties untethered to CNTs,[23] this leads to an average degree of polymerization of 29 TMPM units per grafted chain. Thus, high density grafting with rather long polymer chains are achieved here, benefiting the specific capacity of the resulting composite.
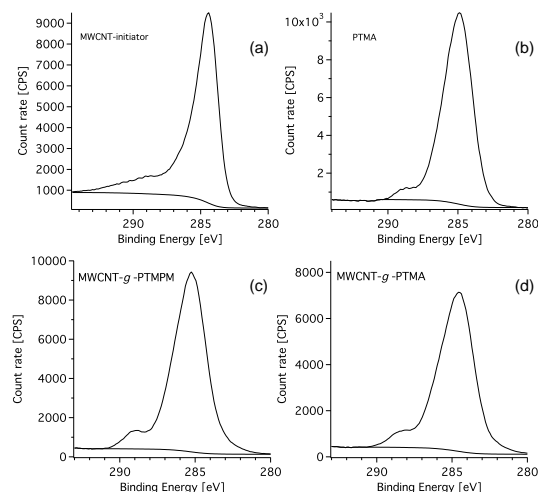
Figure 5. C_{1s} narrow scans of MWCNT-initiator (a), PTMA (b), MWCNT-*g*-PTMPM (c) and MWCNT-*g*-PTMA (d) powder samples.
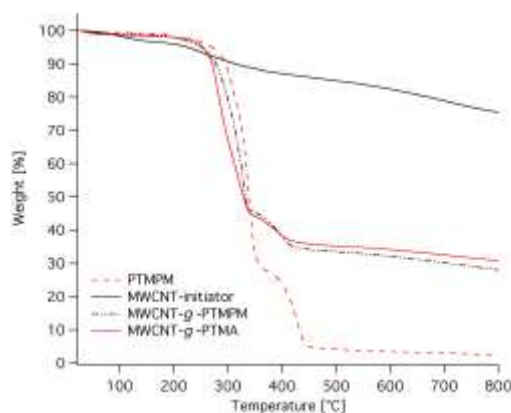
Figure 6. TGA thermograms of pure PTMPM, MWCNT-initiator, MWCNT-*g*-PTMPM and MWCNT-*g*-PTMA. The weight losses between 200°C and 450°C are 95%, 10%, 64% and 65% respectively.

Oxidation of MWCNT-*g*-PTMPM into MWCNT-*g*-PTMA

MWCNT-*g*-PTMPM has been oxidized with a procedure similar to those applied to PTMPM found in the literature.[18] The absence of polymer desorption during oxidation is verified at the end of the process by means of TGA measurements. The thermogram for MWCNT-*g*-PTMA (Figure 6) is affected by a weight loss at a temperature close to the one for the pure PTMA samples.[26] The hybrid material presents the same weight loss

This journal is © The Royal Society of Chemistry 2015

J. Mater. Chem. A, 2015, **00**, 1-3 | **5**

(about 65%) similar to MWCNT-*g*-PTMPM confirming that the polymer is firmly attached to the carbon nanotubes.

More convincingly, XPS analyses deliver atomic concentrations similar for MWCNT-*g*-PTMA and pure PTMA, both close to the expected theoretical values (Table 2). Again the C_{1s} signal (Figure 5d) is consistent with a shell of polymer around the MWCNTs as the curve does not present the typical tail of oxidized CNTs and the shape is more close to the one displayed for pure PTMA (Figure 5b).

Table 2. Experimental surface atomic concentrations for MWCNT-*g*-PTMA compared to experimental and predicted values for pure PTMA.

	Surface atomic concentrations (%)		
	MWCNT-*g*-PTMA	PTMA	
Spectral line	Found	Found	Expected
C_{1s}	80.1	79.3	76.5
O_{1s}	16.1	15.5	17.6
N_{1s}	3.9	5.1	5.9

All these results tend to demonstrate that no significant degradation or elution of the polymer is taking place during the oxidation. Thermal data, chemical compositions and solubility observations are consistent with PTMA covalently anchored at the MWCNT surface.

Electrochemical characterizations

The cathode fabrication process relies on the realization of functionalized MWCNT mats (buckypaper).[27] Practically, pristine MWCNTs dispersed in butanol are first deposited by vacuum filtration to generate a thin film current collector.[27, 28] This layer was also found to allow easy peeling of the electrode at the end of the process. The layer of active material is then obtained by filtration of a MWCNT-*g*-PTMA suspension in *N*-methylpyrrolidone/CH_2Cl_2 6:4 (v/v). The thickness of the fabric after processing was measured to be 86 μm.

Cyclic voltammetry analysis is conducted to assess the redox activity of PTMA (Figure 7). The first cycle reveals a peak centered around 3.6 V *vs.* Li/Li$^+$, which corresponds to the oxidation of the nitroxide radical into an oxoammonium cation.[4]
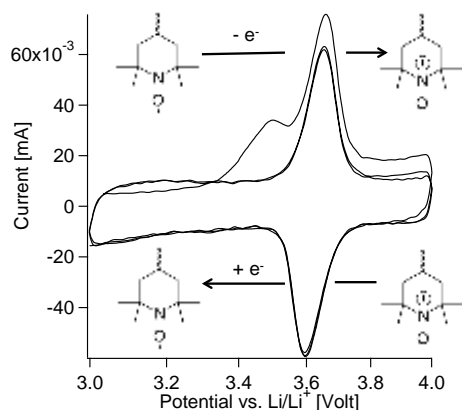
Figure 7. Cyclic voltammogram of MWCNT-*g*-PTMA at 0.1 mV.s^{-1} (EC/DEC/DMC 1:1:1 in v:v:v ; 1 M LiPF$_6$). The 3 first cycles are depicted. Redox reactions associated with positive and negative processes are depicted.

After the first cycle, the successive anodic and cathodic waves display no differences in the redox activity of the electrode, the redox processes being fully reversible with a peak-to-peak separation of 0.06 V.

The electrode capacity retention is evaluated by means of galvanostatic cycling. Figure 8 presents the capacity retention plot versus the number of constant current (220 mA/g) charge/discharge cycles. At the first cycle, a drop in capacity is observed, ascribed to irreversible redox processes. However, the capacity is then stabilized around 80 mAh/g, which corresponds to 72% of the theoretical capacity. The electrodes display excellent capacity retention with less than 13% capacity loss after 200 cycles.
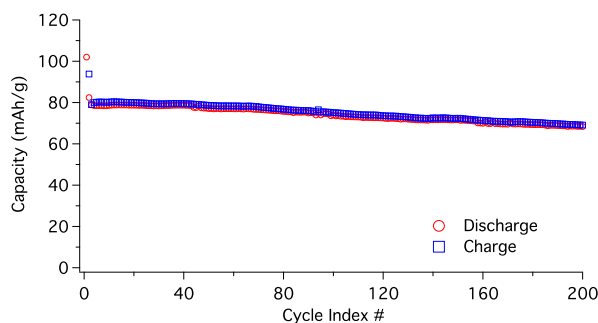
Figure 8. Cycle stability of CNT-*g*-PTMA (60 wt.% PTMA) at 2C rate over 200 cycles.

TGA measurements after cycling experiments demonstrate that no polymer migrates through the electrolyte solution upon cycling. Practically, the cathode after cycling is soaked several times in fresh acetonitrile to remove any Li salt and dried under vacuum. TGA of this cathodic material displays the same composition and degradation profile as the one observed for MWCNT-*g*-PTMA prior cycling (further details are presented in Supplementary Information and Figure S2), evidencing that polymer has not diffused into the electrolyte solution. The degradation mechanism seems then to occur via a different pathway.

The rate capabilities of the cathodes are measured by cycling the electrodes at different current densities (Figure 9). Cycling at C/2 delivers a high reversible capacity of 94 mAh/g (85% of the theoretical capacity). At higher rates, the capacity decreases only slightly. The capacity at 5C is still half of the nominal value obtained at C/2. Furthermore the charge and discharge profiles at 5C maintain the characteristic plateau of PTMA centered at 3.6V (vs. Li/Li+) with slight polarization of about 100 mV (Figure 10) emphasizing the good current collection efficiency of the constructed electrodes. The cathode integrity after the rate capabilities test was measured by cycling the system back to lower current density (C/2). This experiments revealed that the capacity is nearly the same as the one previously observed for the same C-rate.

In order to evidence the benefits of our grafting strategy, control composite electrodes were prepared via the more conventional physical blending of the active (PTMA) and conductive materials (MWCNTs). Details on the preparation of

6 | *J. Mater. Chem. A*, 2015, **00**, 1-3

This journal is © The Royal Society of Chemistry 2015

the control composite are described in the Supplementary Information section. Compared to the MWCNT-*g*-PTMA cyclic voltammogram (Figure 7), the cyclic voltammogram of the control composite electrode (Figure S3) displays a broader peak-to-peak separation (0.08 V), suggesting poorer charge collection efficiency.
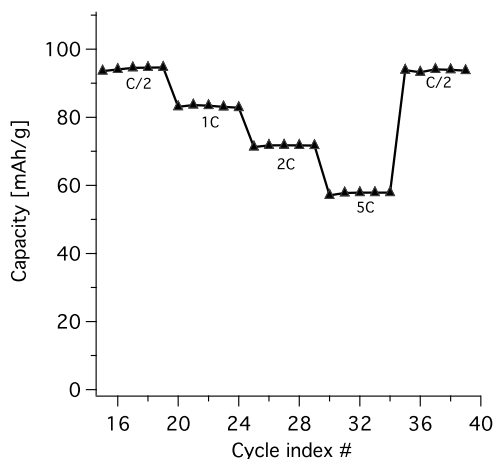
Figure 9. Electrochemical performances of MWCNT-*g*-PTMA (60 wt.% PTMA) cathode at various C rates (EC/DEC/DMC 1:1:1 in volume ; 1 M LiPF$_6$).
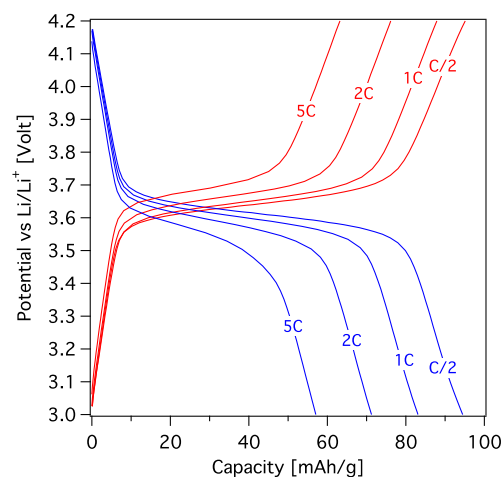
Figure 10. Charge-discharge curves of MWCNT-*g*-PTMA (60 wt.% PTMA) cathode at various C rates (EC/DEC/DMC 1:1:1 in volume ; 1 M LiPF$_6$).

Galvanostatic cycling stability tests on the control composite were also conducted (Figure S4). During the initial conditioning cycling steps, the control electrode displayed a satisfying specific capacity (71 mAh/g). The subsequent cycles were realized with the same current density as with the MWCNT-*g*-PTMA electrodes. The increased current density resulted in dramatic decrease in the capacity retention of the control composite, with as low as 35 mAh/g attained at 220 mA/g (that is 2 times lower than the capacity retention of the grafted material at the same C rate). Moreover, the capacity decay of the control electrode is more pronounced than in the case of the MWCNT-*g*-PTMA electrode. In the latter case, the

electrode displayed a capacity retention as high as 87% whereas the control electrode retained only 78% of its capacity.

Concerning the rate capabilities of the tested electrodes, the performances of the control electrode were again inferior to those obtained with the grafted system (charge-discharges curves are provided in Figure S5). Indeed, the polymer-grafted material displayed superior power performances than the control composite. With respect to common PTMA/conductive carbon blends, the control electrode displayed limited rate capabilities that can be related to its relatively high thickness and high PTMA content. These two parameters are acting here together and result in hampered performances since the redox reactions are not fully supported by the conducting matrix (poor charge transfer due to low carbon content)[8] and because electrode interfacial resistance increases with the thickness.[29] Eventually, for each of the analyzed electrochemical aspect, the comparison plays in favor of the MWCNT-*g*-PTMA electrode. Interestingly, 4 points probe measurements delivered quite close conductivities for the control composite (11.6 S/cm) and our designed system (8.1 S/cm). Thus the enhancement of the rate performances is not arising from a general improvement of the conductivity. A more conceivable explanation must be rather an improvement of the electron transfer between the PTMA and the MWCNTs. Compared to the control composite, the boosted electron transfer in the MWCNT-*g*-PTMA system would then originate from a higher degree of homogeneity at the nano-scale along with a more intimate contact between the active and the conductive components.

Conclusions

The present paper deals with the synthesis of an electrochemically active polymer, the PTMA, covalently anchored onto the surface of MWCNTs. The synthetic strategy successfully involved a controlled grafting from technique, i.e. SI-ATRP, to yield MWCNT-*g*-PTMA with high loading of active material (up to 60 wt.%). TGA, XPS and TEM contributed to characterize the MWCNTs at each step. Particularly these techniques evidenced the nature, the composition and the distribution of grafted materials in the MWCNT-*g*-PTMPM and MWCNT-*g*-PTMA composites.

The MWCNT-*g*-PTMA composite was further processed as a buckypaper electrode via a filtration method. The buckypaper electrode was electrochemically characterized using half-cell configuration with lithium as reference and working electrode. The cycling stability of the designed cathode was evaluated after 200 cycles, demonstrating an excellent capacity retention (87% of the initial capacity is retained). Moreover, during electrochemical measurements, the composite material reached 85% of its theoretical capacity. This high capacity is ascribed to the high conversion of pendant amino groups into nitroxide redox centers during the oxidation step. Variable rate measurements of the electrode additionally attested the ability of the designed electrode to sustain high charge/discharge rates. Altogether the electrochemical characterizations owed to prove

the viability of the accordingly synthetized MWCNT-*g*-PTMA composite as cathodic material for lithium batteries.

Acknowledgements

Notes and references

[a] Institute of Condensed Matter and Nanosciences (IMCN), Bio- and Soft Matter (BSMA), Université catholique de Louvain, Place L. Pasteur 1, B-1348, Louvain-la-Neuve, Belgium.
[b] Information and Communication Technologies, Electronics and Applied Mathematics (ICTEAM) , Université catholique de Louvain , Place de Levant, 3, 1348, Louvain la Neuve , Belgium

Electronic Supplementary Information (ESI) available: XPS atomic concentrations for oxidized MWCNTs and for MWCNT-initiator, XPS Br 3d narrow scan of MWCNT-initiator, TGA of a MWCNT-*g*-PTMA cathode after cycling are available. Details about the preparation of the control electrodes and the results associated (voltammogram, capacity retention plot and variable rate measurements) are also presented. See DOI: 10.1039/b000000x/

1. M. Armand and J. M. Tarascon, *Nature*, 2008, **451**, 652-657.
2. V. Etacheri, R. Marom, R. Elazari, G. Salitra and D. Aurbach, *Energy Environ Sci*, 2011, **4**, 3243-3262.
3. Z. Yang, J. Zhang, M. C. Kintner-Meyer, X. Lu, D. Choi, J. P. Lemmon and J. Liu, *Chem Rev*, 2011, **111**, 3577-3613.
4. T. Janoschka, M. D. Hager and U. S. Schubert, *Adv Mater*, 2012, **24**, 6397-6409.
5. K. Oyaizu and H. Nishide, *Adv Mater*, 2009, **21**, 2339-2344.
6. A. Vlad, N. Singh, J. Rolland, S. Melinte, P. Ajayan and J.-F. Gohy, *Sci Rep*, 2014, **4**.
7. K. Nakahara, J. Iriyama, S. Iwasa, M. Suguro, M. Satoh and E. J. Cairns, *J Power Sources*, 2007, **165**, 870-873.
8. J.-K. Kim, G. Cheruvally, J.-H. Ahn, Y.-G. Seo, D. S. Choi, S.-H. Lee and C. E. Song, *J Ind Eng Chem*, 2008, **14**, 371-376.
9. T. von Werne and T. E. Patten, *J Am Chem Soc*, 1999, **121**, 7409-7410.
10. H. Nishide and T. Suga, *Electrochem Soc Interface*, 2005, **14**, 32-36.
11. S. Y. Iwasa, M. ; Nishi, T. ; Nakano, K., *Nec Tech J*, 2012, **7**, 102-106.
12. K. Nakahara, S. Iwasa, M. Satoh, Y. Morioka, J. Iriyama, M. Suguro and E. Hasegawa, *Chem Phys Lett*, 2002, **359**, 351-354.
13. L. Bugnon, C. J. H. Morton, P. Novak, J. Vetter and P. Nesvadba, *Chem Mater*, 2007, **19**, 2910-2914.
14. A. Vlad, J. Rolland, G. Hauffman, B. Ernould and J.-F. Gohy, *ChemSusChem*, 2015, **10.1002/cssc.201500246**.
15. H.-C. Lin, C.-C. Li and J.-T. Lee, *J Power Sources*, 2011, **196**, 8098-8103.
16. G. Hauffman, Q. Maguin, J.-P. Bourgeois, A. Vlad and J.-F. Gohy, *Macromol Rapid Comm*, 2014, **35**, 228-233.
17. W. Choi, S. Endo, K. Oyaizu, H. Nishide and K. E. Geckeler, *J Mater Chem A*, 2013, **1**, 2999-3003.
18. S. Qin, D. Qin, W. T. Ford, D. E. Resasco and J. E. Herrera, *J Am Chem Soc*, 2003, **126**, 170-176.
19. S. Qin, D. Qin, W. T. Ford, D. E. Resasco and J. E. Herrera, *Macromolecules*, 2004, **37**, 752-757.
20. R. Barbey, L. Lavanant, D. Paripovic, N. Schüwer, C. Sugnaux, S. Tugulu and H.-A. Klok, *Chem Rev*, 2009, **109**, 5437-5527.
21. D. Baskaran, J. W. Mays and M. S. Bratcher, *Angew Chem Int Ed*, 2004, **43**, 2138-2142.
22. A. M. Shanmugharaj, J. H. Bae, R. R. Nayak and S. H. Ryu, *J. Polym. Sci., Part A: Polym. Chem.*, 2007, **45**, 460-470.
23. G. Hauffman, J. Rolland, J.-P. Bourgeois, A. Vlad and J.-F. Gohy, *J. Polym. Sci., Part A: Polym. Chem.*, 2013, **51**, 101-108.
24. V. Mittal, in *Surface Modification of Nanotube Fillers*, Wiley-VCH Verlag GmbH & Co. KGaA, 2011, pp. 1-23.
25. T. I. T. Okpalugo, P. Papakonstantinou, H. Murphy, J. McLaughlin and N. M. D. Brown, *Carbon*, 2005, **43**, 153-161.
26. J.-K. Kim, J.-H. Ahn, G. Cheruvally, G. Chauhan, J.-W. Choi, D.-S. Kim, H.-J. Ahn, S. Lee and C. Song, *Met Mater Int*, 2009, **15**, 77-82.
27. G. Zhou, F. Li and H. M. Cheng, *Energy Environ Sci*, 2014, **7**, 1307-1338.
28. N. Singh, C. Galande, A. Miranda, A. Mathkar, W. Gao, A. L. M. Reddy, A. Vlad and P. M. Ajayan, *Sci Rep*, 2012, **2**.
29. J.-K. Kim, G. Cheruvally, J.-W. Choi, J.-H. Ahn, S. H. Lee, D. S. Choi and C. E. Song, *Solid State Ionics*, 2007, **178**, 1546-1551.

8 | *J. Mater. Chem. A*, 2015, **00**, 1-3

This journal is © The Royal Society of Chemistry 2015